Defect States Emerging from a Non-Hermitian Flatband of Photonic Zero Modes

Bingkun Qi, Lingxuan Zhang, and Li Ge

Defect states emerging from a non-Hermitian flat band of photonic zero modes

Bingkun Qi,[1, 2] Lingxuan Zhang,[1, 3] and Li Ge[1, 2, *]

[1]*Department of Engineering Science and Physics, College of Staten Island, CUNY, Staten Island, NY 10314, USA*
[2]*The Graduate Center, CUNY, New York, NY 10016, USA*
[3]*State Key Laboratory of Transient Optics and Photonics,*
Xi'an Institute of Optics and Precision Mechanics, Chinese Academy of Sciences, Xi'an 710119, China
(Dated: February 6, 2018)

We show the existence of a flat band consisting of photonic zero modes in a gain and loss modulated lattice system, as a result of the underlying non-Hermitian particle-hole symmetry. This general finding explains the previous observation in parity-time symmetric systems where non-Hermitian particle-hole symmetry is hidden. We further discuss the defect states in these systems, whose emergence can be viewed as an unconventional alignment of a pseudo-spin under the influence of a complex-valued pseudo-magnetic field. These defect states also behave as a chain with two types of links, one rigid in a unit cell and one soft between unit cells, as the defect states become increasingly localized with the gain and loss strength.

Defect states are ubiquitous in periodic systems due to the existence of bandgaps. In the simple case of a point defect, if its energy falls deep into a bandgap, then it cannot couple efficiently to the rest of the system, where no propagating mode exists at its energy. As a result, a defect state localized at this point is formed, no matter whether the defect is in the bulk or at the edge of the system. Take the simplest periodic system in one dimension (1D) for example, its unit cell contains one element of energy ω_0 that couples to its nearest neighbors with strength $t > 0$, where a single band extends from $[\omega_0 - 2t, \omega_0 + 2t]$ across the Brillouin zone (BZ). A defect state forms if the on-site energy of a single defect at the edge is detuned from ω_0 by more than t, and it appears above (below) this band if the detuning is positive (negative).

A particular interesting case for defect states is in the presence of a flat band, where a small detuning is sufficient to create a defect state in general. A flat band is dispersionless inside the whole BZ, and systems that exhibit flat bands have attracted considerable interest in the past few years, including optical [1, 2] and photonic lattices [3–6], graphene [7, 8], superconductors [9–12], fractional quantum Hall systems [13–15] and exciton-polariton condensates [16, 17]. Due to the singular density of states at the flat band energy, several interesting localization phenomena and their scaling properties have been identified [18–22].

In Refs. [23–25], parity-time ($\mathcal{PT}$) symmetric perturbations, i.e., those with a complex potential satisfying $V(x) = V^*(-x)$ [26–51], were introduced to study their effects on an existing flat band in the underlying Hermitian system. In the meanwhile, it was known that the introduction of a $\mathcal{PT}$-symmetric potential can collapse two neighboring bands into a single one in terms of their real parts [32], which is flat in some cases [52, 53]. The conditions that lead to this flatness in a non-Hermitian system were poorly understood, and in this work we point out that the mechanism that leads to these flatbands is

actually due to another symmetry, i.e., non-Hermitian particle-hole (NHPH) symmetry [54, 55]. We should mention that similar to the Hermitian case, a non-Hermitian flat band can also exist by engineering a Wannier function that is an eigenstate of the whole lattice (see Sec. I in Ref. [56], which includes Refs. [57–59]).

With NHPH symmetry, the effective Hamiltonian anti-commutes with an antilinear operator, and a particular simple way to achieve it employs a photonic lattice [55]: starting with an underlying Hermitian system with chiral symmetry (also known as sublattice symmetry), which consists of identical elements on two sublattices coupled by nearest neighbor coupling (e.g., a square lattice, honeycomb lattice and so on), NHPH symmetry is automatically satisfied once spatial gain and loss modulation is applied.

The flat band resulted from NHPH symmetry consists of photonic zero modes, which share certain traits as their condensed matter counterparts (i.e., the Majorana zero modes [60–62]). However, these photonic zero modes are not necessarily localized in space, and we study the defect states emerging from these non-Hermitian flat bands by introducing a point defect. We employ the simplest 1D photonic lattice mentioned before but now with gain and loss modulation that doubles or quadruples the size of the unit cell. We show that a flat band is formed when the gain and loss strength γ exceeds a critical value. Now by introducing a point defect at the edge of the system, a defect state appears and becomes increasingly localized as the non-Hermiticity of the system increases. This defect state behaves as a chain with two types of links, one rigid within a unit cell and one soft between unit cells. We find that the emergence of the defect state can be viewed as an unconventional alignment of a pseudo-spin under the influence of a complex-valued pseudo-magnetic field, and in some cases, the result of a $\mathcal{PT}$ transition. These results are first discussed using a tight-binding model and then verified by ab-initio vector simulations of Maxwell's equations in photonics waveguides.

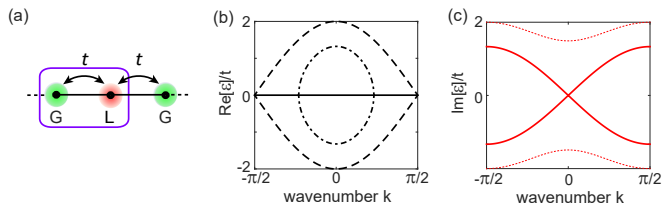*Non-Hermitian Flat Band* — The periodic system we

FIG. 1. (Color online) (a) Schematic of a gain and loss modulated lattice with period $m = 2$. The box indicates the unit cell. (b) and (c) Real and imaginary parts of the bands in (a). The dashed lines in (b) mark the Hermitian bands when $\gamma = 0$. The dash-dotted line show their partial collapse when $\gamma = 1.5t$. The solid line shows the completed flat band when $\gamma \geq 2t$. The solid and dotted lines in (c) are for $\gamma = 2t$ and $3t$, respectively.

consider is the simplest 1D lattice mentioned in the introduction, and we choose the identical on-site energy of the lattice sites to be the zero point of its energy levels. With the introduction of gain and loss modulation, the non-Hermitian system can be captured by the tight-binding model

$$i\partial_t \psi_n = i\gamma_n \psi_n + t(\psi_{n-1} + \psi_{n+1}) \quad (n = 1, 2, \ldots). \quad (1)$$

Below we consider a periodic imaginary potential with $\gamma_n = \gamma_{n+m}$ where m is an even integer. For an odd m the system does not have two sublattices and hence NHPH symmetry does not hold.

When the period m equals 2 [see Fig. 1(a)], the effective Hamiltonian can be written in the following form, by dropping an offset of the imaginary potential:

$$H_2 = \begin{bmatrix} i\gamma & t(1 + e^{-2ik}) \\ t(1 + e^{2ik}) & -i\gamma \end{bmatrix}. \quad (2)$$

γ here is defined as $(\gamma_n - \gamma_{n+1})/2$, and we have set the distance between two neighboring lattice sites to be 1. The dispersion relations of this system are then given by $\varepsilon_{\pm}(k) = \pm\sqrt{2t^2(1 + \cos 2k) - \gamma^2}$ in the BZ $k \in [-\pi/2, \pi/2)$. This effective Hamiltonian satisfies

$$\{H_2, \mathcal{CT}\} = 0, \ [H_2, \mathcal{PT}] = 0, \quad (3)$$

i.e., it has both NHPH symmetry and $\mathcal{PT}$ symmetry (see Sec. II in Ref. [56]). Here $\mathcal{T}$ is the time-reversal operator in the form of the complex conjugation, and the chiral operator $\mathcal{C} = \sigma_z$ and parity operator $\mathcal{P} = \sigma_x$ are given by the Pauli matrices. The curly and square brackets denote anti-commutation and commutation relations as usual.

We note that $\mathcal{PT}$ symmetry dictates that the bands of the system satisfy $\varepsilon_i(k) = \varepsilon_j^*(k)$, where i, j are band indices. In the case that i, j are different, the two bands have the same Re$[\varepsilon]$ but different Im$[\varepsilon]$, which was a result of spontaneous $\mathcal{PT}$ symmetry breaking [27]. Nevertheless, $\mathcal{PT}$ symmetry does not ensure that their identical Re$[\varepsilon]$ needs to be flat in the BZ, and in Ref. [32] this merged band was indeed found to be curved.

NHPH symmetry, on the other hand, leads to a band structure satisfying $\varepsilon_i(k) = -\varepsilon_j^*(k)$ instead [55]. It clearly indicates that when $i = j$, a flat band at Re$[\varepsilon] = 0$ can emerge with photonic zero modes. For the $m = 2$ case above, this flat band starts to emerge from the boundary of the BZ as soon as γ is nonzero, and it is formed completely when $\gamma > \gamma_c \equiv 2t$ [see Fig. 1(b)]. In Sec. III of Ref. [56] we show another example where $m = 4$ and the system lacks $\mathcal{PT}$ symmetry; the existence of a non-Hermitian flat band in this case corroborates the role of NHPH symmetry.

Defect States — Having shown that NHPH symmetry leads to a non-Hermitian flat band, next we probe the defect states emerging from it. One example is shown in Fig. 2(a) where a defect of detuning Δ is introduced to the left edge of the system (now of a finite length). We note that the defect state is formed at a small Δ as a result of the flat band, which is in contrast to the Hermitian case (e.g., the simplest 1D lattice) we have mentioned in the introduction.

One interesting feature of the defect state is its staggered intensity profile on the log scale [Figs. 2(c) and (d)]: if we define the unit cells by counting from the $n = 2$ site (i.e., avoiding the defect at the left edge), the intensity ratio R within each unit cell is a constant for all unit cells. The same is true for the intensity ratio R' between the gain (loss) sites in two neighboring unit cells. Based on
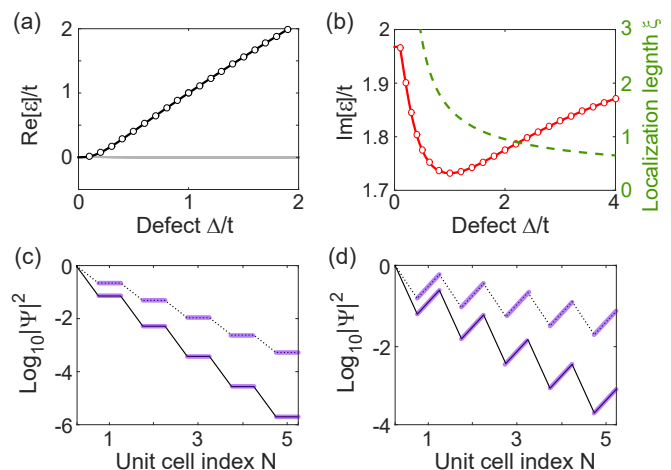

FIG. 2. (Color online) Emergence of a defect state from a non-Hermitian flat band as a function of the defect detuning Δ, where the period of the gain and loss modulation is $m = 2$. (a) and (b) Real and imaginary parts of the defect state energy as a function of the detuning Δ. The solid lines and the dots show numerical results and the analytical expression (4), respectively. $\gamma = 2t$ is used. In (a) the grey lines show the almost unperturbed flat band energies of the bulk modes. In (b) the dashed line shows the localization length of the defect state. (c) Intensity profile of the defect state with $\Delta = t$. $\gamma = 2t\,(1.3t)$ for the solid (dotted) line. Only the left 5 unit cells are shown (marked by the "rigid links" that are parallel and γ-independent). (d) Same as (c) but with $\Delta = t/2$. $\gamma = 2t\,(1.1t)$ for the solid (dotted) line.

these observations, we derive an analytical expression for ε_Δ of the defect state in Sec. IV of Ref. [56]:

$$\varepsilon_\Delta = \frac{(t^2 + \Delta^2) \mp \sqrt{(t^2 - \Delta^2 - 2i\gamma\Delta)^2 + 4t^2\Delta^2}}{2\Delta}, \quad (4)$$

where the "$-(+)$" sign should be used for $\Delta < t\,(\Delta > t)$. This expression agrees nicely with the numerical data in Figs. 2(a) and 2(b).

Furthermore, we find that the intra-cell intensity ratio R mentioned above is simply given by

$$R = \frac{\Delta^2}{t^2} \quad (5)$$

and *independent* of the non-Hermitian parameter γ. In the meanwhile, the inter-cell intensity ratio R' is given by

$$R' = \frac{\Delta^4}{t^4} \left| \frac{\varepsilon_\Delta + i\gamma}{\varepsilon_\Delta - i\gamma} \right|^2, \quad (6)$$

which does vary with γ. Therefore, the defect state behaves as a chain with two types links as we increase the non-Hermiticity of the system via γ, one rigid within a unit cell and one soft between unit cells. This observation also indicates that the wave function of the defect state is exponentially localized on both sublattices [Figs. 2(c) and (d)], with the *same* localization length given by $\xi = 4/\ln R'$. At first glance this result may seem counterintuitive because one would expect that the intensity of the wave will be amplified on the gain lattice sites and attenuated on the loss lattice sites, which will result in a varying inter-cell intensity ratio along the lattice and different localization lengths on the gain and loss sublattices. However, we remind the reader that here gain and loss do not describe wave propagation along the lattice. It is most obviously in a photonic lattice consisting of parallel waveguides, where the gain and loss characterizes wave propagation along the waveguides. We also note that the localization length is not directly related to $\mathrm{Im}[\varepsilon_\Delta]$. The latter is determined simultaneously by R and R', which lead to a non-monotonic Δ-dependence of $\mathrm{Im}[\varepsilon_\Delta]$ [see Fig. 2(b)]; the localization length, on the other hand, reduces monotonically as Δ increases.

Another interesting question about the defect state is how it evolves from the underlying Hermitian system as γ increases and the flat band is formed. As Figs. 3(a) and 3(b) show, the defect state originates from the middle of the Hermitian band, especially when Δ is small. By inspecting Eq. (4), we find that $|\Delta| = t$ is a special case, where a $\mathcal{PT}$ transition takes place at $\gamma = t$. We note that this is a different $\mathcal{PT}$ transition from those that take place on the real-ε axis when the flat band is formed. We also note that Eq. (4) applies only when the defect state is localized and has a staggering intensity profile. Therefore, it is not surprising that its prediction in Fig. 3(a) [and Fig. 3(b)] deviates from the numerical result when γ is small and the defect state is still in the bulk (see Sec. V
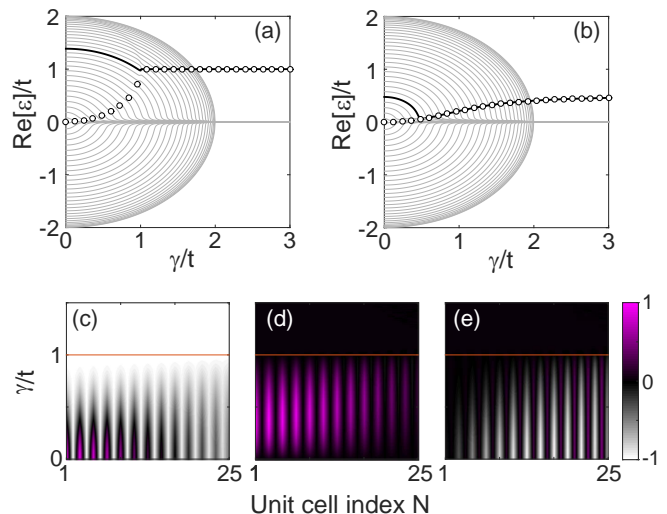

FIG. 3. (Color online) Emergence of a defect state from a non-Hermitian flat band as a function of the gain and loss strength γ with period $m = 2$. (a) and (b) Real part of all the modes in the system (solid lines) with $\Delta = t$ and $t/2$, respectively. The black line indicates the evolution of the defect mode, and the circles are the prediction of Eq. (4). (c)–(e) False color plots of the pseudo-spin $\langle \sigma \rangle_{x,y,z}$ as a function of position and γ in (a). Only the left 25 unit cells are shown.

in Ref. [56]). Nevertheless, the $\mathcal{PT}$-broken phase of ε_Δ in $\gamma > t$, characterized by its γ-independent real part, is faithfully manifested by the numerical data.

Now if we inspect the spatial profile of the defect state as it evolves with γ, we observe an unconventional alignment of a pseudo-spin under the influence of a complex-valued pseudo-magnetic field. To be more specific, we first rewrite the effective Hamiltonian (2) using the Pauli matrices:

$$H_2 = t(1 + \cos ka)\,\sigma_x - t\sin ka\,\sigma_y + i\gamma\,\sigma_z \equiv -\boldsymbol{h} \cdot \boldsymbol{\sigma}, \quad (7)$$

where $\boldsymbol{h}(\gamma) = [-t(1+\cos ka),\, t\sin ka,\, -i\gamma]$ is our complex-valued pseudo-magnetic field. We normalize the wave function $[\psi_L, \psi_G]^T$ in each unit cell when calculating $\langle \boldsymbol{\sigma} \rangle$, and the result is plotted in Figs. 3(c)–(e) as a function of γ when $\Delta = t$. It is clear that $\langle \boldsymbol{\sigma} \rangle$ displays a spatially dependent orientation when $\gamma < t$, but an aligned $\langle \boldsymbol{\sigma} \rangle$ is found across the whole lattice when $\gamma > t$. This value of $\langle \boldsymbol{\sigma} \rangle$ is given by $(-1, 0, 0)$ and can be viewed as the result an unconventional alignment of a pseudo-spin, since the direction of a complex $\boldsymbol{h}$ cannot be uniquely defined. The same alignment process takes place for other values of Δ as well. For example, $\langle \boldsymbol{\sigma} \rangle$ becomes $[-0.8, 0, -0.6]$ when $\Delta = t/2$. We note that $\langle \sigma \rangle_y$ is always zero in the aligned state; it is in fact proportional to the optical flux between the gain and loss sites [63] in a unit cell by definition [i.e., $i(\psi_G^* \psi_L - \psi_G \psi_L^*)$], which vanishes as one can show that $\psi_L/\psi_G = -\Delta/t$ is real (whose square gives R). Using this ratio we also derive $\langle \sigma \rangle_x = -2\Delta t/(\Delta^2 + t^2)$, $\langle \sigma \rangle_z = (\Delta^2 - t^2)/(\Delta^2 + t^2)$, which agree nicely with

their aforementioned numerical values (see also Sec. VI in Ref. [56]).

Photonic realization — Next we present a realistic design using coupled photonic waveguides to demonstrate the practical feasibility of the predicted effects given above. Each waveguide has a square cross section, which is 1.5 μm wide and has a 500-nm-thick InGaAsP mutiple quantum wells on top of an InP substrate [see Fig. 4(a)]. When optically pumped, the quantum wells supply the gain while the loss can be provided, for example, by a thin Cr/Ge double layer on top of the quantum wells that also blocks the pump. Similar structures have been used in a number of experimental demonstrations with fine controlled gain and loss ratios [64, 65]. The propagating mode along the waveguide direction can be denoted by $\vec{\Psi}(x,y,z) = \vec{E}(x,y)e^{-i\beta z}$, where $\vec{E}$ is the vector electric field. The propagation distance z and propagation constant β now play the roles of time and the eigenvalue ε of the effective Hamiltonian, respectively.

Below we introduce the effective index $n_{\text{eff}} = \beta\lambda/2\pi$ to characterize each propagating mode, with the wavelength chosen at $\lambda = 1.55\mu$m. By performing a finite-difference-time-domain simulation of Maxwell's equations using MEEP [66] and a perfectly matched layer as the global boundary condition, we find $n_{\text{eff}} = 3.25 \equiv n_0$ for the fundamental mode in a single waveguide [see Fig. 4(b)]. With two coupled waveguides separated by 0.2 μm, we find that the two corresponding n_{eff}'s now differ by 1.17×10^{-4}, indicating a dimensionless coupling constant $t = 5.83 \times 10^{-5}$. Now if we consider 20 waveguides, their individual fundamental modes couple to form a band with bandwidth $\Delta n_{\text{eff}} = 2.31 \times 10^{-4}$, which agrees
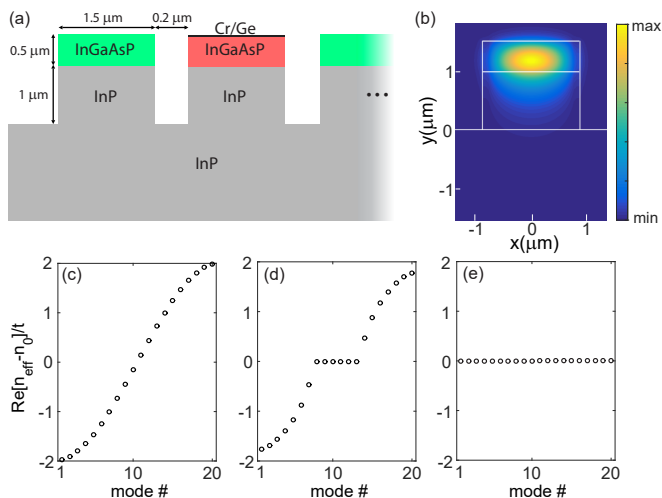

FIG. 4. (Color online) (a) Schematic of coupled photonic waveguides with alternate gain and loss. The refractive indices used are 3.17 (InP), $3.44 + in''$ (InGaAsP), and $3.44 - in''$ (Cr/Ge + InGaAsP). (b) $|E_x|$ component of the fundamental mode in a single waveguide when $n'' = 0$. (c)–(f) Real part of the band structure when $n'' = 0, t, 2t$.
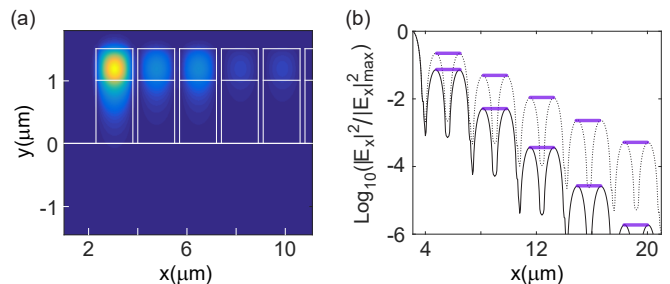

FIG. 5. (Color online) A defect state with a staircase profile. (a) Same as Fig. 4(b) but with 20 coupled waveguides and $n'' = 2t$. The refractive index of the left waveguide is now increased by $\delta n = 7.43 \times 10^{-5}$. (b) Its staggering profile at $n'' = 2t$ (solid line) and $1.3t$ (dotted line). $|E_x|$ is taken at $y \approx 1.2\,\mu$m where it is maximized. The horizontal "rigid links" from Fig. 2(c) are reproduced here and the agreement is excellent.

well with the tight-binding prediction ($4t$) mentioned in the introduction [see Fig. 4(c)]. By increasing gain and loss incorporated as the imaginary part n'' of the top layer(s) that plays the role of the non-Hermitian parameter γ, we illustrate the forming of the non-Hermitian flat band in Figs. 4(e) and 4(f) when n'' is increased to $2t$, again verifying the prediction of the tight-binding model. Furthermore, we introduce a "point defect" similar to Fig. 2 by including an index detuning $\delta n = 7.43 \times 10^{-5}$ in the gain layer of the left waveguide, which can be achieved, for example, by placing a layer of Ge on top of the waveguide [64, 65] (see also Sec. VII in Ref. [56]); it results in a change of the single-waveguide n_{eff} by t, and we recover the staircase mode profile that displays an n''-independent "rigid link" inside a unit cell and an n''-dependent "soft link" between unit cells (see Fig. 5).

Conclusion and Discussion — In summary, we have shown that NHPH symmetry can lead to a flat band consisting of photonic zero modes, which explains the previous finding in $\mathcal{PT}$-symmetric systems where NHPH symmetry is hidden. Although we have only examined 1D lattices here, this mechanism also applies in higher dimensions (see Sec. VIII in Ref. [56], which includes Ref. [67]). The defect states emerging from this flat band exhibit several interesting properties, such as possessing two types of links, one rigid within a unit cell and one soft between unit cells, as the defect states become increasingly localized with the non-Hermitian parameter. These behaviors, first predicted using a tight-binding model, have been verified by full vector simulations of Maxwell's equations for the propagation modes in coupled photonic waveguides.

The emergence of these defect states can be viewed as an unconventional alignment of a pseudo-spin under the influence of a complex-valued pseudo-magnetic field, and in certain cases, the result of a $\mathcal{PT}$ transition. We note that for this pseudo-spin in our photonic lattice, spin-spin

and spin-orbital interactions are absent and difficult to introduce, hence they are not considered here.

———————

* li.ge@csi.cuny.edu

[1] V. Apaja, M. Hyrkäs, and M. Manninen, Phys. Rev. A **82**, 041402(R) (2010).

[2] M. Hyrkäs, V. Apaja, and M. Manninen, Phys. Rev. A **87**, 023614 (2013).

[3] M. C. Rechtsman, J. M. Zeuner, A. Tünnermann, S. Nolte, M. Segev, and A. Szameit, Nat. Photon. **7**, 153 (2013).

[4] R. A. Vicencio, C. Cantillano, L. Morales-Inostroza, B. Real, C. Mejía-Cortés, S. Weimann, A. Szameit, and M. I. Molina, Phys. Rev. Lett. **114**, 245503 (2015).

[5] S. Mukherjee, A. Spracklen, D. Choudhury, N. Goldman, P. Öhberg, E. Andersson, and R. R. Thomson, Phys. Rev. Lett. **114**, 245504 (2015).

[6] M. Biondi, E. P. L. van Nieuwenburg, G. Blatter, S. D. Huber, and S. Schmidt, Phys. Rev. Lett. **115**, 143601 (2015).

[7] C. L. Kane and E. J. Mele, Phys. Rev. Lett. **78**, 1932 (1997).

[8] F. Guinea, M. I. Katsnelson, and A. K. Geim, Nat. Phys. **6**, 30 (2010).

[9] A. Simon, Angew. Chem. **109**, 1873 (1997).

[10] S. Deng, A. Simon, and J. Köhler, Angew. Chem. **110**, 664 (1998).

[11] S. Deng, A. Simon, and J. Köhler, J. Solid State Chem. **176**, 412 (2003).

[12] M. Imada and M. Kohno, Phys. Rev. Lett. **84**, 143(2000).

[13] E. Tang, J-W. Mei, and X-G. Wen, Phys. Rev. Lett. **106**, 236802 (2011).

[14] T. Neupert, L. Santos, C. Chamon, and C. Mudry, Phys. Rev. Lett. **106**, 236804 (2011).

[15] S. Yang, Z.-C. Gu, K. Sun, and S. Das Sarma, Phys. Rev. B **86**, 241112(R) (2012).

[16] T. Jacqmin et al., Phys. Rev. Lett. **112**, 116402 (2014).

[17] F. Baboux et al., Phys. Rev. Lett. **116**, 066402 (2016).

[18] J. T. Chalker, T. S. Pickles, and P. Shukla, Phys. Rev. B **82**, 104209 (2010).

[19] J. D. Bodyfelt, D. Leykam, C. Danieli, X. Yu, and S. Flach, Phys. Rev. Lett. **113**, 236403 (2014).

[20] D. Leykam, S. Flach, O. Bahat-Treidel, and A. S. Desyatnikov, Phys. Rev. B **88**, 224203 (2013).

[21] S. Flach, D. Leykam, J. D. Bodyfelt, P. Matthies, and A. S. Desyatnikov, Europhys. Lett. **105**, 30001 (2014).

[22] L. Ge, Ann. Phys. (Berlin) 527, 1600182 (2017).

[23] L. Ge, Phys. Rev. A **92**, 052103 (2015).

[24] G.-W. Chern and A. Saxena, Opt. Lett. **40**, 5806 (2014).

[25] M. I. Molina, Phys. Rev. A **92**, 063813 (2015).

[26] C. M. Bender and S. Boettcher, Phys. Rev. Lett. **80**, 5243 (1998).

[27] C. M. Bender, S. Boettcher, and P. N. Meisinger, J. Math. Phys. **40**, 2201 (1999).

[28] C. M. Bender, D. C. Brody, and H. F. Jones, Phys. Rev. Lett. **89**, 270401 (2002).

[29] R. El-Ganainy, K. G. Makris, D. N. Christodoulides, and Z. H. Musslimani, Opt. Lett. **32**, 2632 (2007).

[30] S. Klaiman, U. Gunther, and N. Moiseyev, Phys. Rev. Lett. **101**, 080402 (2008).

[31] Z. H. Musslimani, K. G. Makris, R. El-Ganainy,

[32] K. G. Makris, R. El-Ganainy, D. N. Christodoulides, and Z. H. Musslimani, Phys. Rev. Lett. **100**, 103904 (2008).

[33] A. Guo, G. J. Salamo, D. Duchesne, R. Morandotti, M. Volatier-Ravat, V. Aimez, G. A. Siviloglou, and D. N. Christodoulides, Phys. Rev. Lett. **103**, 093902 (2009).

[34] A. Mostafazadeh, Phys. Rev. Lett. **102**, 220402 (2009).

[35] T. Kottos, Nat. Phys. **6**, 166 (2010).

[36] S. Longhi, Phys. Rev. A **82**, 031801(R) (2010).

[37] Y. D. Chong, L. Ge, and A. D. Stone, Phys. Rev. Lett. **106**, 093902 (2011).

[38] P. Ambichl, K. G. Makris, L. Ge, Y. Chong, A. D. Stone, and S. Rotter, Phys. Rev. X **3**, 041030 (2013).

[39] L. Ge, Y. D. Chong, and A. D. Stone, Phys. Rev. A **85**, 023802 (2012).

[40] L. Ge, K. G. Makris, D. N. Christodoulides, and L. Feng, Phys. Rev. A **92**, 062135 (2015).

[41] L. Ge and A. D. Stone, Phys. Rev. X **4**, 031011 (2014).

[42] L. Ge and R. El-Ganainy, Sci. Rep. **6**, 24889 (2016).

[43] Z. Lin, H. Ramezani, T. Eichelkraut, T. Kottos, H. Cao, and D. N. Christodoulides, Phys. Rev. Lett. **106**, 213901 (2011).

[44] C. E. Rüter, K. G. Makris, R. El-Ganainy, D. N. Christodoulides, M. Segev, and D. Kip, Nat. Phys. **6**, 192 (2010).

[45] A. Regensburger, C. Bersch, M. A. Miri, G. Onishchukov, D. N. Christodoulides, and U. Peschel, Nature (London) **488**, 167 (2012).

[46] S. Bittner, B. Dietz, U. Günther, H. L. Harney, M. Miski-Oglu, A. Richter, and F. Schäfer, Phys. Rev. Lett. **108**, 024101 (2012).

[47] L. Feng, Y.-L. Xu, W. S. Fegadolli, M.-H. Lu, J. E. B. Oliveira, V. R. Almeida, Y.-F. Chen, and A. Scherer, Nat. Mater. **12**, 108 (2013).

[48] L. Feng, Z. J.Wong, R.-M.Ma, Y.Wang, and X. Zhang, Science **346**, 972 (2014).

[49] H. Hodaei, M. A. Miri, M. Heinrich, D. N. Christodoulides, and M. Khajavikhan, Science **346**, 975 (2014).

[50] B. Peng et al., Nat. Phys. **10**, 394 (2014).

[51] L. Chang et al., Nat. Photon. **8**, 524 (2014).

[52] B. Zhu, R. Lü, and S. Chen, Phys. Rev. A **89**, 062102 (2014).

[53] H. Zhao, S. Longhi, and L. Feng, Sci. Rep. **5**, 17022 (2015).

[54] S. Malzard, C. Poli, and H. Schomerus, Phys. Rev. Lett. **115**, 200402 (2015).

[55] L. Ge, Phys. Rev. A **95**, 023812 (2017).

[56] See the Supplemental Material.

[57] A. V. Yulin and V. V. Konotop, Opt. Lett. **38**, 4880 (2013).

[58] H. Ramezani, Phys. Rev. A **96**, 011802 (2017).

[59] D. Leykam, S. Flach, and Y. D. Chong, Phys. Rev. B **96**, 064305 (2017).

[60] J. Alicea, Rep. Prog. Phys. **75**, 076501 (2012).

[61] C. W. J. Beenakker, Rev. Mod. Phys. **87**, 1037 (2015).

[62] S. D. Sarma, M. Freedman, and C. Nayak, npj Quantum Information **1**, 15001 (2015).

[63] L. Ge, K. G. Makris, and L. Zhang, Phys. Rev. A **96**, 023820 (2017).

[64] P. Miao, Z. Zhang, J. Sun, W. Walasik, S. Longhi, N. M. Litchinitser, and L. Feng, Science **353**, 464 (2016).

[65] Z. J. Wong, Y.-L. Xu, J. Kim, K. OBrien, Y. Wang, L. Feng, and X. Zhang, Nat. Photon. **10**, 796 (2016).

[66] http://ab-initio.mit.edu/wiki/index.php/Main_Page (accessed on October 13, 2017).

[67] W.A. Harrison, Phys. Rev. **118**, 1190 (1960).